Oxygenic and anoxygenic photosynthesis in a microbial mat from an anoxic and sulfidic spring.

Dirk de Beer[1*], Miriam Weber[2], Arjun Chennu[1], Trinity Hamilton[4], Christian Lott[2], Jennifer Macalady[5], Judith Klatt[1,3]

*corresponding author, dbeer@mpi-bremen.de

[1]Max-Planck-Institute for Marine Microbiology, Microsensor Group, Celsiusstrasse 1, 28215 Bremen, Germany

[2]HYDRA Institute for Marine Sciences, Via del Forno 80, Fetovaia, 57034 Campo nell'Elba (LI), Italy

[3]Geomicrobiology Laboratory, Dept. of Earth & Environmental Sciences, University of Michigan, Ann Arbor, MI 48109, USA

[4]Department of Biological Sciences, University of Cincinnati, Cincinnati, OH 45221, USA

[5]Department of Geosciences, Pennsylvania State University, University Park, PA 16802, USA

running title: Benthic phototrophy in a Proterozoic analog

Originality/significance statement

The Little Salt Spring sinkhole is an anoxic ecosystem that is used as analog for the Proterozoic world, before and during the great oxidation event (GOE). At the lake bottom, red cyanobacterial mats cover sediments full of green sulfur bacteria. Previous community studies of the mat are complemented by this study of the biogeochemical processes. Oxygenic and anoxygenic photosynthesis rates were measured *in situ* and in the laboratory using microsensors. The combination of *in situ* and laboratory measurements complement physiological findings by molecular and culturing methods. We found evidence for direct transfer of radiation energy up to 1 cm deep in the mats, although the *in situ* quality and intensity of the radiation is unfavorable for photosynthesis. We also found that iron cycling in such mats has a profound effect on photosynthesis. Oxygen evolution occurs in a layer less than 1 mm thick during 4 hours per day, yet this is enough to support aerobic microorganisms. This type of microbial ecosystem was possibly the first aerobic environment on early Earth, in which the biochemical tools were developed to survive and flourish in an oxygenated world.

Summary

Oxygenic and anoxygenic photosynthesis were studied with microsensors in microbial mats found at 9-10 m depth in anoxic and sulfidic water in Little Salt Spring (Florida, USA). The lake sediments were covered with a 1-2 mm thick red mat dominated by filamentous Cyanobacteria, below which Green Sulfur Bacteria (GSB, Chlorobiaceae) were highly abundant. Within 4 mm inside the mats, the incident radiation was attenuated to undetectable levels. *In situ* microsensor data showed both oxygenic photosynthesis in the red surface layer and light-induced sulfide dynamics up to 1 cm depth. Anoxygenic photosynthesis occurred during all daylight hours, with complete sulfide depletion around midday. Oxygenic photosynthesis was limited to 4 hours per day, due to sulfide inhibition in the early morning and late afternoon. Laboratory measurements on retrieved samples showed that oxygenic photosynthesis was fully but reversibly inhibited by sulfide. In patches Fe(III) alleviated the inhibition of oxygenic photosynthesis by sulfide. GSB were resistant to oxygen and showed a low affinity to sulfide. Their light response showed saturation at very low intensities.

Introduction

Modern phototrophic ecosystems that are dominated by bacteria and archaea are often considered as analogs for the ecology of the early Earth. Studies on such modern communities will help to interpret chemical and isotopic signals in stromatolites, and other fossils to provide insight into these early stages of life and the evolution of the Earth (Canfield and Teske, 1996; Habicht and Canfield, 1996; Knoll et al., 2007). The great oxidation event (GOE, 2.4 Ga ago) was accompanied by profound global changes in sulfur and iron cycling (Canfield, 1998). Canfield argued that the GOE occurred in two oxygenation steps: the first led to increased weathering and increased sulfate levels which enhanced sulfate reduction and led to iron removal by sulfide precipitations; and the second step led to full oxygenation of the atmosphere and deep oceans. Cyanobacteria are the only bacteria that can perform oxygenic photosynthesis, and many strains can also perform anoxygenic photosynthesis. It is likely that both anoxygenic and oxygenic photosynthesis were already in operation before the GOE.However, the potential rate of oxygen production was likely lower than the input of reductants into the biosphere by volcanism (Canfield, 2013). Any oxygen that was produced was rapidly consumed rendering the biosphere anoxic. Even under these reducing conditions there might have been oxygenation events in microenvironments of microbial mats long before the oxygenation of oceans. Microbial mats are cohesive microbial communities with cell densities several orders of magnitude higher than in the water column. Light quality and intensity structures phototrophic mats vertically in laminae of distinct metabolic groups of microorganisms, with Cyanobacteria as the dominant primary producer. The ensuing high volumetric metabolic rates, together with mass transfer limitations, induce steep gradients of substrates and products. Therefore, the concentrations of oxidants and reductants in microbial mats can profoundly differ from those in the water column. We investigated if microbial mats in sulfidic environments can perform oxygenic photosynthesis.

Multicellular organisms developed following the GOE and as a result, mats became limited to the uncommon environments where grazers are excluded. The most intensively investigated mats are found in hypersaline or hot environments (Stolz and Margulis, 1984; Bateson and Ward, 1988; Jørgensen and Des Marais, 1988; Canfield and Des Marais, 1991; Ferris et al., 1997; Ramsing et al.,

2000; Wieland and Kühl, 2000; Hoehler et al., 2002; Nübel et al., 2002; Wieland et al., 2005; Klatt, 2015). More recently, an interest has developed for hypoxic or anoxic environments at the bottom of sinkholes that are influenced by seeping groundwater(Hamilton et al., 2016a; Voorhies et al., 2016). The seeping groundwater is devoid of oxygen and enriched in sulfur species, which leads to the formation of dense microbial mats at the bottom of these lakes. Little Salt Spring (Florida, USA) is of moderate temperature, low in salinity, hypoxic (<30% airsaturation) and slightly sulfidic (Clausen et al., 1979). The apparent sulfur cycling (sulfate is 5 mM, sulfide is 40 μM) would make the lake an analog for the oceans just before or during the GOE (Canfield, 1998). The bottom of the upper basin is covered by red microbial mats. A recent study (Hamilton et al., 2016b) showed that these are dominated by Cyanobacteria and GSB (*Chlorobium* spp). Remarkably, the most common Cyanobacteria could be cultivated and several of its physiological characteristics were determined, showing that they can perform both oxygenic photosynthesis and anoxygenic photosynthesis and that sulfide inhibits oxygenic photosynthesis (Klatt, 2015). Our aim was to assess if these characteristics are reflected in the behavior of the consortium from which they were isolated. Green sulfur bacteria perform only anoxygenic photosynthesis using thiosulfate, sulfide, S(0), Fe^{+2} or H_2 (Overmann and Garcia-Pichel, 2012), and are sensitive to oxygen (Harada et al., 2005). Thus the interplay between the two communities is complex. We investigated the mats with microsensors for oxygen, pH and H_2S both *in situ* and under controlled conditions in the laboratory. We investigated if both oxygenic and anoxygenic photosynthesis occur, whether both processes occur simultaneously, what their vertical distributions are, whether sulfide inhibits oxygenic photosynthesis, and whether the mats can form a net source of oxygenation.

Results

Site, mat structure and appearance

The red mats carpet coarse sandy sediments in the upper basin of Little Salt Spring. Microscopic examination showed that the top 0.5-1.5 mm consist of a cohesive layer of red filamentous cyanobacteria (with a diameter of approximately 5 µm), below which green masses filled the pore-spaces (Fig. 1). The green mass in the sediments consisted of amorphous clusters of single cells which were identified previously as Chlorobiaceae, or Green Sulfur Bacteria (GSB) (Hamilton et al., 2016b). Motile white filaments resembling *Beggiatoa* were observed occasionally on top of the red mat. The filaments had a diameter of 5-10 µm and contained sulfur granules. No metazoans, such as nematodes or tardigrades, were observed in extensive microscopic examinations.

The water column below 3 m depth contained approximately 40 µM total sulfide, nitrate was not detected, pH decreased from 7.6 at the surface to 7.3 at 10 m depth and then stayed constant, temperature decreased from 27°C at the surface to 26.7°C at 7-10 m depth and then stayed constant, and salinity was constant at 0.3 %. While oxygen was, incorrectly, detected by CTD, microsensors indicated the water column to be anoxic where the red mat is observed. The outflow of the spring is 42.8 L s^{-1} (Clausen et al., 1979), thus with a volume of approximately 140000 m^3 the water column has a residence time of ~40 days. SCUBA divers observed some circulation along a transect crossing the sloping upper basin and the sinkhole orifice using injected milk plumes. In the center of the orifice an upflow of approximately 1 cm s^{-1} was observed, and on the slopes, a downwelling was observed with approximately the same flow velocity.

In situ radiation

Radiation spectra indicate the presence of Bacteriochlorophyll (BChl) -c, -d, -e or -f (Stomp et al., 2007; Croce and van Amerongen, 2014)(Stomp et al., 2007; Croce and van Amerongen, 2014) in the water column at 2 m intervals; however, no Chlorophyll-a (Chl-a) fluorescence was detected. In the upper water column, the absorbance spectrum showed peaks at 475 and 720 nm (Supplementary Information Fig. S1). As red and infrared radiation became quickly attenuated the absorbance spectra

at 3 and 5 m depth could not resolve the peak at 720 nm, but showed the peak of 475 nm. The light intensity at the mat surface during midday varied between 50-75 µmol photons $m^{-2}s^{-1}$. Its spectrum ranged from 450-700 nm and had a maximum at 570 - 580 nm (Supplementary Information Fig. S2A). Thus the radiation reaching the mats had very little blue and no red components. Radiation profiles were measured inside the mats, showing that most attenuation occurred within the 0.5-1 mm depth interval (Fig. 2A). Radiation between 450 and 600 nm was absorbed in this layer, and a Chl-a peak at 670 nm was observed. Radiation was detectable up to 3-4 mm depth with wavelengths above 600 nm (Fig. 2B; Supplementary Information, Fig. S2). Below 1.5 mm depth radiation levels were too low to calculate accurate absorbance values above 600 nm.

Ex situ light profiles

In retrieved mats that were illuminated with a halogen lamp, radiation also attenuated rapidly with depth. In contrast to the *in situ* radiation, this lamp produced also red, infrared and blue components. Downwelling irradiance of 60 µmol photons $m^{-2}s^{-1}$ attenuated almost completely within 2 mm in the mat.

The wavelength-specific attenuation visible in the spectral profiles measured under PAR illumination at 60 µmol photons $m^{-2}s^{-1}$ provide information on the vertical distribution of photopigments (Fig. 2C, Supplementary Information Fig. S2B). At 0.5 and 1 mm depth a Chl-a absorbance peak at 670 nm is present and strong absorbance occurs between 450 and 600 nm, probably by antennae pigments. At 2 mm depth a peak is visible at 805 nm, possibly of BChl-a. In the upper 1.5 mm radiation of the shorter wavelengths (<700 nm) attenuated much stronger than that of longer wavelengths and blue radiation became completely depleted. Below 2 mm depth red radiation attenuated further, but at a lower rate than the blue radiation in the red layer. Similar results were obtained with a downwelling radiation intensity of 10 µmol photons $m^{-2}s^{-1}$. The profiles can be explained by the structure of the mat. The red upper layer consists of Cyanobacteria, which effectively absorb the shorter wavelengths (450-600 nm) for oxygenic photosynthesis, while infra-red radiation penetrates deeper and can be used by anoxygenic phototrophs below the red mat (Fig.1).

In situ chemical microprofiles

Two successful deployments of the diver operated microprofiler (DOMS) each for 24 hours resulted in continuous recordings of O_2 and H_2S microprofiles. The pH profiling was unsuccessful, so that the dynamics of H_2S could not be converted to S_{tot} dynamics. In addition, no changes were detected in the absence of light (at night) so only the data from 06:00-18:00 h are presented. From the series of O_2 and H_2S microprofiles contours plots were constructed which demonstrate the distributions of oxygen and sulfide in response to the changing light levels due to the movement of the sun and irregularly passing clouds (Figs. 3A, 4A). Remarkably, net oxygenic production (Fig. 3B) occurred only during a few hours per day, between 10:00 and 15:00 h, whereas a decrease in H_2S occurred during the entire light period, from 7:30-17:30 h (Fig. 4A, B). The H_2S dynamics at 1 cm depth were simultaneous with the radiation dynamics at the surface of the mats (Fig. 4B).

In situ oxygen sensor data show that the mats are growing in an anoxic environment. The previously reported hypoxia (Clausen et al., 1979), defined as 1-30% of air saturation, may be due to contamination of anoxic samples by air. During the period of oxygen production, 0.2 µM oxygen was detected in the water column just above the mat surface. This value was obtained by averaging the water column oxygen signals measured 1-3 mm above the mats over 3 hours during midday, and comparing these with the signals recorded during midnight and in the anoxic deeper zone. The water column near the mats was anoxic during the remaining time (before 10:00 and after 15:00 h). Sulfide remained constant in the water column, independent of illumination.

O_2 and H_2S profiles, representative for light and dark conditions, were averaged from 5 profiles each (Fig. 5). Under illumination, oxygen developed within the mats due to oxygenic photosynthesis. The highest net photosynthesis (RO_2 in Fig. 5C) occurred at 0.5 mm depth and respiration continued down to 3 mm depth (Fig. 5C). In the light sulfide was consumed at a depth of 4 mm, whereas in the dark sulfide diffused up to the surface (Fig. 5B). Although radiation intensity decreased below detection limit at 4 mm depth (Fig. 1B), a decrease of sulfide under illumination was observed to 1 cm depth. Due to missing pH profiles, S_{tot} could not be quantified and no total sulfide fluxes could be calculated.

However, in the light the H_2S gradient between 1 and 4 mm depth was about half of the gradient

present in the dark. This means that the upward diffusive sulfide flux in the light is lower than in the

dark.

Ex situ chemical microprofiles

Our CTD data showed oxygen to be present at 50% of air saturation at the depth where mats were

sampled and as a result, incubations of retrieved mats were performed under oxic conditions to reflect

in situ conditions. However, upon analysis of the *in situ* microprofiles described above, it became

clear that the CTD data were wrong and the ambient water column is anoxic. Despite a homogeneous

appearance of each mat and similarity in color and structure of the samples, the pH and H_2S

microprofiles were variable and appeared in two categories: either sulfide reached the surface in the

dark or it was depleted in the upper few mm. In three out of seven samples sulfide reached the

surface in the dark (Type 1), while in the other four samples no sulfide was detected in the upper mat

(Type 2). The O_2 and H_2S profiles in samples of Type 1 and 2 are displayed in the Supplement

(Supplementary Information, Fig. 3 and 4).

Complete sets of microprofiles (O_2, pHand S_{tot}) in the Type 1 mats are presented in Fig. 6. In the dark,

oxygen penetrated 200-300 μm and overlapped with sulfide. Upon illumination with an intensity

close to ambient (60 μmol photons $m^{-2}s^{-1}$), oxygen accumulated in the upper 2 mm whereas sulfide

receded below the mat to deeper in the core. In the light sulfide and oxygen never overlapped,

indicating that sulfide was consumed by anoxygenic photosynthesis and not by aerobic sulfide

oxidation. In the light, the fluxes were $JO_{2(out)}$ 1.7×10^{-6} mol $m^{-2}s^{-1}$, $JO_{2(down)}$ 1×10^{-6} mol $m^{-2}s^{-1}$. In the

light JS_{tot} was 8.4×10^{-9} mol $m^{-2}s^{-1}$, which is one order of magnitude lower than in the dark (7.2×10^{-8}

mol $m^{-2}s^{-1}$). Similar as observed *in situ*, sulfide levels decreased very deep in the mats upon

illumination. The dark fluxes were JO_2 2.2×10^{-7} mol $m^{-2}s^{-1}$ and JS_{tot} 7.2×10^{-8} mol $m^{-2}s^{-1}$. Thus, similar

to the pattern observed *in situ*, the diffusive upward flux of sulfide in the upper cm was higher in the

dark than in the light. The distribution of conversion rates (Fig. 6C and D) showed that sulfide

consumption in the dark co-occurs with oxygen consumption. In the light, the zones of oxygen and sulfide consumption are separate, at 2-3 mm and 4-6 mm respectively.

In Type 2 mat samples the sulfidic and oxic zone were separated by of several mm in the dark (Fig. 7A), indicating a sulfide oxidizing process. Also in the light, oxygen and sulfide did not overlap. Oxygen production was confined to the upper 1-2 mm (Fig. 7B). Light reduced the upward sulfide flux in the upper 8 mm. In the dark, strongly enhanced sulfide levels in the water column were necessary to observe penetration of sulfide into the mat (Fig. 7C). A likely oxidant could be Fe(III), which could have accumulated during the day (Wieland et al., 2005). Fe^{2+} oxidation could have occurred by oxygen that was photosynthetically produced by the cyanobacteria or directly by light driven oxidation by GSB. Indeed, using two methods to determine reduced and oxidized iron showed strongly elevated levels, especially of Fe(III), in the red mat (Table 1).

Oxygenic photosynthesis was inhibited by very low levels of sulfide. In Type 2 mat samples, oxygenic photosynthesis developed very quickly in the upper 1 mm. Experimental elevation of S_{tot} in the water column from natural levels to 1 mM caused only slightly enhanced sulfide levels in the photic zone of the mat (<25 μM S_{tot} and < 1 μM H_2S). However, this low level of sulfide instantly stopped oxygenic photosynthesis (Supplemental Information, Fig. S5). At the location where the downward diffusing sulfide was consumed a strong pH peak developed (Supplementary Information, Fig. S5B), indicating a reaction of sulfide with Fe(III) (Preisler et al., 2007). The inhibition was reversible, when sulfide in the overlaying water was reduced to ambient levels (40 μM), oxygen production instantly recovered (data not shown).

Sulfide kinetics was studied by positioning pH and H_2S sensors at a fixed position in the mats to measure sulfide dynamics upon darkening and illumination (Supplementary Information, Fig. S6). The consumption of sulfide upon illumination was much faster than sulfide production upon darkening. Sulfide consumption gradually increased upon illumination to a maximum consumption rate in 30-60 seconds, after which it decreased again due to kinetic limitation. We used this maximum sulfide consumption rate as an estimate for the gross rate of anoxygenic photosynthesis. After the

maximum, the consumption rates were proportional to the concentration (Supplementary Information Fig. S7) following first order kinetics ($R=k \times C$) (Levenspiel, 1972). The depth distribution of gross anoxygenic photosynthesis was determined using dark-light shifts. At 60 µmol photons $m^{-2} s^{-1}$ anoxygenic photosynthesis was remarkably constant between 2 and 6 mm depth (Fig. 8). Anoxygenic photosynthesis did not decrease with depth and thus seems not to be controlled by radiation intensity, meaning the GSB are light-saturated down to 6 mm depth. At 10 and 30 µmol photons $m^{-2} s^{-1}$ depth independent sulfide consumption could be detected until 3 mm and 5.5 mm depth, respectively.

In the determination of the gross anoxygenic photosynthesis by dark-light shifts, sulfide production due to sulfate reduction can be ignored, as it is much lower than the consumption (Fig 8B). Sulfide production was determined by first removing all sulfide by illumination and subsequently darkening the mats, while H_2S and pH profiles were continuously measured. The local rates of S_{tot} increase were calculated and found to be ~1 % of the sulfide consumption rates (Fig. 8A).

The dark-light shifts were used to determine PI curves at 2 mm depth (Supplementary Information, Fig. S8). Saturation of the consumption rates were obtained at a surface radiation intensity of 30-40 µmol photons $m^{-2} s^{-1}$. As radiation is attenuated strongly (Fig. 2D), we corrected the PI curve accordingly (upper x-axis in Fig S6.) and found that saturation occurred at local radiation intensity of 0.2 µmol photons $m^{-2} s^{-1}$.

Discussion

Energy availability in LSS and mat morphology

In a previous study of the red mats, the dominant populations were found to be Cyanobacteria and GSB based on clone library and pigment analyses (Hamilton et al., 2016b), but the vertical distribution of organisms in the mat was not investigated. Our microscopy showed the upper red skin to consist of Cyanobacteria and GSB were observed in the sediments below. The stratified structure of the mat community was confirmed by spectral signatures captured at different depths within the mat: a thin layer of Cyanobacteria overlying masses of GSB that preferentially absorb longer wavelengths. *In situ* incident radiation occurred mainly in the 450-700 nm region, with a strong attenuation above 600 nm. Our *in situ* spectral measurements show that nearly all of this radiation is dissipated/attenuated within the top 1.5-2 mm of the mat; but this does not preclude anoxygenic photosynthesis from occurring because GSB can grow in extremely low light environments (Overmann et al., 1992). Most *in situ* radiation is between 500 and 600 nm, a wavelength range that forms a minimum in the photosynthetic action spectrum of both oxygenic and anoxygenic phototrophs (McConnell et al., 2002; Falkowski and Raven, 2007). Cyanobacteria use the accessory pigments phycoerythrin, phycocyanin and allophycocyanin (Klatt, 2015) to harvest radiation in the 500-650 nm range (Nichols and Bogorad, 1962; Glazer, 1985). The found antennae pigment isorenieratene allow the GSB to harvest radiation between 350 and 500 nm (Overmann et al., 1992) which overlaps somewhat with the light quality we observed.

Oxygen production

From the series of profiles we conclude a total absence of oxygen at night and a very subtle increase of 0.2 µM in the water column during midday. Although oxygen was released by the microbial mats, it did not accumulate in the reduced water column. The lake chemistry is unique as light penetrates through the sulfidic watercolumn to the mats, and is not attenuated by a dense stratum of anoxygenic phototrophs as is commonly observed in other euxinic systems. We found evidence for Bchl through specific absorption at 720 nm (Fig. S1), thus some light-driven sulfide consumption likely occurs in

the water column. However, the observed currents of 1 cm s^{-1} are sufficient to overturn the anoxic water column several times per day, dissipating gradients in sulfide that could be induced by anoxygenic photosynthesis, and maintaining stable sulfide levels in the water column above the mats. Also the mixing prevents development of a layer of anoxygenic phototrophs near the chemocline, thus enabling light to penetrate to the mats in the upper basin.

The *in situ* oxygen and sulfide microprofile measurements were done on two successive days, however, they were performed in close proximity (within 1 cm) and the radiation regime was comparable. Sulfide dynamics and radiation correlated well. Throughout the entire period of sunlight (from 7:30 h till 17:00 h) the sulfide concentration decreased. Sulfide was not immediately depleted upon the start of the illumination and only after several hours (after 10:00 h) was complete sulfide depletion observed at 0.5 mm depth. After 15:00 h sulfide was again detectable over the whole depth profile. Conversely, radiation and oxygen levels did not correlate very well. Oxygen production was limited to a period from 10:00 h to 15:00 h. In this period, variations in radiation intensities, due to passing clouds, were reflected in O$_2$ levels. Thus, in addition to light, sulfide also controlled oxygenic photosynthesis, as oxygenic photosynthesis occurs only when sulfide is fully depleted. It should be noted that the depth where sulfide depletion occurred was occupied by Cyanobacteria. This observation indicates that the Cyanobacteria in the red mat switch smoothly from H$_2$S to H$_2$O as electron source for CO$_2$ fixation when H$_2$S is depleted. In our laboratory measurements oxygenic photosynthesis did not occur in the presence of detectable sulfide and sulfide inhibition was rapidly reversible. These findings match earlier results from detailed physiological studies of isolates of the most abundant Cyanobacterial strain from these mats (Klatt, 2015).

The anoxic and illuminated upper basin of Little Salt Spring may be considered as an analog to the habitat of the early Earth during the long period after oxygenic photosynthesis had developed, but when the biosphere was not yet oxygenated. Whereas the water column is persistently anoxic, oxygen production by the red microbial mats leads to very local accumulation of oxygen during a part of the day. It is possible that such small zones were the only aerobic environments for the approximate one billion years after the 'invention' of oxygenic photosynthesis and before the great oxidation event.

These photosynthetic microenvironments may have been the source of the 'whiffs' of oxygenation (Anbar et al., 2007; Canfield, 2013) that preceded the large scale oxidation events. It can be assumed that, similar to Little Salt Spring mats, O_2 diffusing out of such aerobic microenvironments was quickly consumed in the strongly reduced surrounding world. Such oxygenated micro-zones may have existed for many hundreds of millions years on a strongly reduced Earth (Canfield, 2013). In such small and ephemeral oxygenated pockets the biochemical tools must have been developed that were needed to survive and exploit the eventually oxygenated world. Directly following the onset of the GOE, organisms equipped with these tools were able to spread and control global element cycling. For instance we observed aerobic sulfide oxidizing *Beggiatoa* on top of the mats. They rely on the oxygen produced by the cyanobacterial mats and the sulfide from the water column. Nitrate, an alternative electron acceptor for Beggiatoa, was not detected in the water column (detection limit 0.16 µM). Further studies on the presence and activities of aerobic heterotrophic and autotrophic communities in these mostly anoxic microenvironments may be rewarding.

Deep anoxygenic photosynthesis

We assumed oxygen production would force the GSB deeper in to the mat and decrease their exposure to light. Instead, we observed the GSB to be regularly exposed to oxygen and instantly capable of anoxygenic photosynthesis when anoxia and sulfide levels were restored, indicating that these GSB can survive temporary oxygen exposure and do not have to perform a balancing act between oxygen inhibition and light limitation. This is consistent with previous observations of GSB in presumed oxic zones in Yellowstone hot spring mats (Liu et al., 2012).

We employed dark-light shifts to measure gross anoxygenic photosynthesis. However, how reliably light perturbation methods can measure photosynthesis can be a matter of debate. The responses were not instant; it took 0.5-1 minute before the sulfide consumption was maximal. Conversely, also light-dark shifts showed a lag-period. Regardless, we assume that the occurrence of light-induced dynamics confirms the presence of anoxygenic photosynthesis, and are proportional to its rate.

Anoxygenic photosynthesis rates measured by dark-light perturbations (Fig. 9) were constant with depth, and appeared not to be dependent on the radiation intensity. The GSB were thus light-saturated in the upper 6 mm. This was confirmed in the PI-curve where saturation was observed at very low radiation levels, below 0.2 μmol photons m^{-2}s^{-1}. This light level was reached at 4-5 mm depth, at 6 mm light intensity was below 0.1 μmol photons m^{-2}s^{-1}. From the dark-light perturbation, we derived that the reaction was first order to sulfide meaning that the Km was far above 100 μM. This is an unusually low affinity to an essential substrate. However, reported values for GSB are highly divergent, possibly reflecting properties of different strains and/or used light intensities. For instance, van Gemerden reported values ranging from 1-54 μM in 17 isolates, measured on suspensions of different isolates under saturating light (~300 μmol photons m^{-2}s^{-1})(van Gemerden, 1984). Findlay et al report a value of 11 μM in dilute suspensions exposed to an irradiance of 5 μmol photons m^{-2}s^{-1} (Findlay et al., 2015). In an engineering study of a very dense (0.5 mm thick) GSB biofilm exposed to an radiation of 6 μmol photons m^{-2}s^{-1}, a saturation of the sulfide conversion was found at 300 μM. The high density of the biofilm must have resulted in a very strong attenuation of radiation with depth. In Little Salt Spring, our evidence indicates that the GSB in the mats have a low affinity to sulfide, with a Km that must exceed 0.1 mM, a very high affinity to light, and a distribution of activity to a depth where little or no light penetrates.

We observed steady state sulfide consumption at 5 mm depth where the radiation level was only 0.3 μmol photons m^{-2}s^{-1} (Fig. 2D). Generally, sulfide diffusing upwards disappeared at depths with radiation intensities well below 1 μmol photons m^{-2}s^{-1}. To estimate the quantum yield (mol photons mol^{-1} sulfide consumed) the ratio of the radiation- and sulfide fluxes were calculated from 8 steady state profiles measured at 30 or 60 μmol photons m^{-2}s^{-1} downwelling irradiance. The radiation fluxes at the depth where sulfide was consumed were 0.3 $\pm$0.1 μmol photons m^{-2}s^{-1}, the sulfide fluxes averaged $3 \pm 1.3 \times 10^{-8}$ mol m^{-2}s^{-1}, resulting in a quantum yield of 12$\pm$7 mol photons mol^{-1} sulfide, or a quantum yield for sulfide of 0.08. The reported quantum yield for CO_2 is in the range of 0.02-0.3, depending on the wave length of the radiation and the organism (Oren et al., 1977; Brune, 1989). The stoichiometry of CO_2:H_2S can vary between 0.5 and 2, depending on the product (S(0) or SO_4^{-2}). Thus

the quantum yield calculated from the radiation and sulfide flux at 4 mm depth is at a realistic order of magnitude. Yet, the problem remains that sulfide seems to be consumed below the photic zone.

Based on the overlapping *in situ* O_2 and H_2S profiles in the light it might be concluded that sulfide consumption is entirely aerobic and that oxygen produced is immediately consumed by sulfide oxidation. The diel cycles in oxygen and sulfide distributions show that sulfide is consumed from sunrise to sunset, and oxygen is only present during 5 hours around midday. However, sulfide at 10 mm depth, well below the oxic zone of the upper 4 mm, followed closely the radiation dynamics at the mat surface. Sulfide consumption occurred far below the zone where radiation is measurable. During the day the sulfide level at 1 cm was half the concentration that occurs at night. The H_2S dynamics at 10 mm depth cannot be explained with diffusive transport towards a micro-oxic zone. The diffusion time is obtained from the distance to the oxygen producing zone at 0.5 mm depth (9.5 mm) and the diffusion coefficient (1.6×10^{-9} m^2 s^{-1}) (Berg, 1983). Upon the start of oxygen production and thus aerobic oxidation of sulfide, it would take 9 hours for the sulfide decrease in the oxic zone to have an effect at 1 cm depth. Thus the H_2S dynamics at 1 cm depth cannot be attributed to light-driven oxygen production in the photic zone and ensuing sulfide consumption, followed by diffusion to 1 cm depth. Instead, anoxygenic photosynthesis may have been responsible for the sulfide dynamics but this explanation is complicated. The *in situ* radiation spectrum below 4 mm depth was indistinguishable from the background noise. The diffusive transport from 4 mm depth to 10 mm depth is still far too slow (t_D = 3 hours) to explain why the sulfide dynamics at 10 mm depth follow the radiation regime so closely. A explanation for this observation may be analogous to the concept of cable bacteria (Nielsen et al., 2010), that were shown to couple oxygen reduction at the sediment surface to sulfide oxidation at a depth of several cm in the sediment. Possibly, oxidizing power generated in the surface layer can accept electrons directly from such a distance by similar cables. The electrons would then be donated to these cables at some depth by bacteria, e.g. GSB, that receive the electrons from sulfide.

Together, several of our observations are unexpected and invite further study: 1) anoxygenic photosynthesis rates remained mostly constant until 6 mm depth, although most of the radiation

intensity was attenuated strongly with depth; 2) the observation that sulfide dynamics occur deeper and are faster than can be explained by radiation or diffusive transport, respectively; 3) sulfide is consumed in the dark. The latter will be discussed in the following.

Non-photosynthetic sulfide consumption

The dynamics and fluxes in Little Salt Springs cannot be described simply by the interplay of oxygenic and anoxygenic phototrophic communities, and sulfide consumption and production processes. The separation between the oxic and sulfidic zone, as regularly observed during laboratory measurements (Fig. 7), demonstrates that sulfide and oxygen consumption are not always coupled. The downward oxygen flux in these mats is not driven by aerobic sulfide oxidation. Instead, the e-donor could be sulfur, Fe^{2+} or photosynthetically formed organics. The diffusive sulfide flux in the light was 10 times lower than in the dark and the upward diffusing sulfide disappeared deep below the oxic zone. Thus, light energy must penetrate far below the oxic zone, where it lowers the sulfide levels and thereby reduces the sulfide flux in the upper cm. Also in Type 1 mats, with overlapping oxygen and sulfide gradients in the dark, the oxygen flux was higher than can be expected from sulfide oxidation (Fig. 6). When sulfide is fully oxidized to sulfate, two oxygen molecules are consumed per sulfide ($2HS^- + 4 O_2 -> 2SO_4^{2-} + 2H^+$). As the measured stoichiometry was even higher (Fig. 6, ratio of the dark fluxes $O_2:S_{tot}=3.1$), oxygen must be used for other oxidation processes than of sulfide.

In the dark, aerobic sulfide oxidation was rarely observed, as the oxic and sulfidic zones were often separated. Even in the dark, sulfide could be lower in the mats than in the water phase (e.g. Fig. 7) indicating sulfide consumption that is not driven by oxygen or light. The strong sulfide consumption in the dark can be explained by the presence of oxidized iron. Fe levels were found to be elevated in the photic zone (Table 1). The accumulation of Fe(III) could result from a combination of factors including abiotic oxidation of Fe^{2+} by O_2, precipitation of dust or biological oxidation of Fe^{2+} by anoxygenic photosynthesis. Assuming a mat porosity of 0.9 and ensuing density of 1.07, the Fe(III) content was 3.5-4 mol m^{-3}, or assuming a mat thickness of 3 mm approximately 0.01 mol m^{-2}. This

amount is sufficient to absorb the typical sulfide fluxes ($0.3\text{-}1 \times 10^{-7}$ mol m^{-2} s^{-1}) for several days. A phototrophic mat surrounded by a sulfidic environment will accumulate iron, since all iron that enters the mat will be trapped either as iron sulfide or as iron oxide. GSB are known to quickly oxidize sulfide to elemental sulfur when illuminated (Imhoff, 2014). Obviously, the presence of such solid phase 'redox buffers' of sulfur and Fe(III) complicates the interpretations of microsensor profiles and fluxes towards processes. More importantly, Fe(III) accumulations in the photic zone would provide oxygenic phototrophs a crucial advantage as only they can be active in the Fe(III)-rich zone where the geochemistry is dominated by an effective sulfide scavenger. Possibly, Fe(III) accumulations stimulated the development of oxygenic photosynthesis, which required habitats where alternative e-donors were depleted. Such an accumulation of Fe(III) in a strongly reduced environment is only possible due to mass transfer resistance. This tempting scenario would make mats crucial in the evolution of oxygenic photosynthesis.

Implications

Our data on the interplay between oxygenic and anoxygenic photosynthesis do not provide a novel explanation on the delay of oxygenation after development of photosynthesis. Little Salt Spring represents rather the scenario where the global supply of reductant, due to tectonics, exceeds the potential for photosynthesis (Knoll et al., 2007; Canfield, 2013). In Little Salt Spring, the mixing of the anoxic part of the water column prevents sulfide depletion in the photic zone and thus effectively suppresses oxygenic photosynthesis. Our study provides an addition to the scenario where high reductant input suppresses oxygen evolution in the ancient ocean, despite phototropic activity (Canfield, 2013): even if oxygenic photosynthesis is inhibited in the water column, it could develop in microbial mats, in which transport resistance limited reductant supply needed for anoxygenic photosynthesis. Iron may have played a crucial role in the oxygenation of the world: by shielding sulfide from the photic zone, iron cycling can force a system from anoxygenic- to oxygenic photosynthesis. Iron will accumulate in the photic zone, thus it has a strong control on these two modes of photosynthesis mats.

The lake represents a unique ecosystem to study the survival of aerobic microorganisms in a largely anaerobic world. Oxygen is present in very short intervals, in an extremely narrow zone that is regularly exposed to toxic sulfide. To study which species can indeed survive such a stress is relevant from an evolutionary perspective. Finally, the phenomenon that sulfide dynamics occur very deep in the mats, below the photic zone requires further study.

Methods

The experiments and sampling were performed from Nov. 4-10, 2014 at Little Salt Spring in North Port, Florida. Laboratory experiments were performed in facilities available on site. Little Salt Spring is a sink hole in karstic rock in Sarasota County, FL (lat. 27°04'30"N, long. 82°14'00"W). The geology and hydrology of the spring have been described elsewhere (Zarikian et al., 2005). The surface is circular with a diameter of 80 m and the depth of the lake is 77 m. At 15 m depth the diameter is reduced to approximately 30 m. Below this depth there are several ledges below which the sinkhole widens again. The shallow areas (2 m depth) are densely covered with green alga (Chara spec.). Between 4 - 13 m depth the sloping bottom is completely covered with red microbial mats. The water column was reported to be hypoxic below 3 m depth and sulfidic (Clausen et al., 1979).

The upper 6-10 cm of sediment, covered with the red microbial mat, was sampled by SCUBA diving at 9-11 m water depth using plexiglass cores with a diameter of 5 cm and a length of 15 cm. The cores were brought to the lab and stored in the dark at 25-28 ˚C for less than 12 hours before they were used in experiments.

Water column data were obtained by a CTD deployed from a platform at the approximate center of the sinkhole. Water depth, temperature, conductivity, Chl-a fluorescence, and oxidation–reduction potential (ORP) were measured *in situ* using a calibrated multiparameter YSI 6600 probe (Yellow Springs, OH, USA). Dissolved sulfide concentrations were measured spectrophotometrically by the methylene blue method for total sulfides (Hach method 690, detection limit 2 μM) using a portable spectrometer (Hach Co., Loveland, CO). Dissolved nitrate was measured in the field using a portable spectrophotometer with the Cadmium Reduction method (detection limit of 0.16 μM; Hach Co.,

Loveland, CO, USA). Water column samples were collected using a 3.8 L Van Dorn bottle (Wildlife Supply Company, Yule, FL) and were analyzed immediately for sulfide concentrations as they were brought to the surface. Sulfide analyses were conducted in duplicate and the values were within 5 % of each other. Radiation intensity distribution was measured using a using a scalar quantum PAR sensor (LiCor LI-193S, Lincoln, NE, USA) attached to a data logger (LiCor LI-1400, Lincoln, NE, USA). Diurnal *in situ* radiation dynamics were recorded with an Odyssey Integrating PAR Sensor (Dataflow Systems Pty. Limited) that was calibrated *in situ* with the LiCor LI-193S. Radiation spectra in the water column and within the mats were measured using a fiber optic spherical irradiation sensor (100 μm diameter) connected to an Ocean Optics USB2000 spectrometer in a water-proof housing (Wangpraseurt et al., 2014; Rickelt et al., 2016). Absorbance spectra were calculated per depth interval as the logarithmic difference of the spectral intensities between the upper and lower interval boundaries. Irradiance profiles were calculated by integrating the spectral intensities between 400-800 nm, and calibrating the surficial irradiance as measured by the LiCor PAR sensor.

Microsensors for O_2, H_2S and pH were prepared, calibrated and used as described previously (Revsbech and Ward, 1983; Jeroschewski et al., 1996; de Beer et al., 1997). In the laboratory the sensors were positioned at the mat surface by using a dissection microscope, to determine the sediment-water interface or zero '0' position. Microsensor profile measurements were performed using a micromanipulator equipped with a stepper-motor. Usually 2 sensors were used simultaneously on two separate micromanipulators. The mats were illuminated by either white light halogen lamps (Schott 2500).

For *in situ* microsensor measurements, a diver operated motorized microsensor profiler (Diver Operated Microsensor System, DOMS) was used (Weber et al., 2007). The DOMS performs stepwise single microsensor profiling of selected parameters (O_2, H_2S, pH) within sediments and mats. The DOMS was also used for measurements of radiation penetration into the mats using the fiber-optic radiation sensor described above (Wangpraseurt et al., 2014). Absorbance spectra in the mats were calculated as explained above for the water column. The DOMS was deployed to record series of profiles with H_2S and O_2 microsensors during 24 hour periods, to assess the vertical dynamics of

chemistry during a diel cycle. The exact positions of the tip of the microsensors relative to the surface were determined under water by using a magnifying glass and a strong lamp. For positioning at the surface the sensor manipulated until the shadow from the lamplight of the sensor on the mat and the sensor optically touched. To avoid shadowing of the investigated spot, the equipment was positioned so that the stands were behind the sensors in the light path. A small fraction of the diffuse light is blocked, due to the amplifier holding the microsensor. From the diameter of the amplifier is (3 cm) and its distance to the sensor tip (17 cm) we calculated that this effect is < 1%.

Total sulfide (S_{tot}) was calculated from the H_2S concentration and pH value using a pK of 6.7 (Millero et al., 1988).

Fluxes (J) were calculated from concentration gradients using Fick's law of diffusion with D_{eff} the effective diffusion coefficient in the mats, C the concentration of the solute and x the distance. D_{eff} was obtained from the molecular diffusion coefficient in water corrected for the salinity (0.3%) and the reduction of diffusivity in mats (65% (Wieland et al., 2001)), resulting in D_{eff} for O_2 of 1.6×10^{-9} $m^2\ s^{-1}$ and for S_{tot} of $1.04 \times 10^{-9}\ m^2\ s^{-1}$. Volumetric conversion rates, i.e. production or consumption, were calculated using a 1-D approach, from the differences in fluxes between two depths (Gieseke and de Beer, 2004).

Using dark-light shifts, gross anoxygenic photosynthesis rates were determined as the maximum rate of S_{tot} consumption upon illumination.

Iron contents were determined on mats that were separated into the red skin and the underlying 1 cm of coarse sediment with green biomass. The samples were stored in -20°C, freeze dried and powdered. Of this material, 50 mg aliquots were used in two separate chemical extractions and finally Fe content analyses. One aliquot was sequentially extracted with 10 ml 1 M sodium acetate solution (pH 4.5) and 10 ml 1 M sodium dithionite-citrate solution (pH 4.8) under an N_2 atmosphere (Henkel et al., 2016). The other aliquot was extracted with 10 ml 2.5N HCl for 2.5 hrs. All extracts were filtered through 0.2 µm membrane filters. Total Fe and Fe(III) were measured immediately after filtration using the 'Hach FerroVer' and the 'Ferrous Iron kit', respectively (Hach Co., Loveland, CO, USA). The sodium acetate treatment extracts reduced Fe, such as adsorbed Fe, Fe-bound carbonates and acid-volatile

sulfides. The sodium dithionite-citrate treatment extracts the remaining Fe(III) (Henkel et al., 2016). HCl treatment extracts all of the aforementioned Fe fractions, including some Fe in silicates (Raiswell et al., 1994).

Table 1.   Fe content of the mats and the sediments below the mats. Values are in mg Fe per gram dry weight. The analysis was done with two different approaches on samples that were split in two aliquots. In one aliquot Fe was extracted by HCl, that was then analysed for Fe^{2+} and total Fe, the difference was taken as Fe(III). The second aliquot was subjected to sequential extraction by Na-acetate (Fe^{2+}) and by dithionate-citrate (extract the remaining Fe(III)), and each were analysed for total Fe.

	HCl-extraction		Na-acetate	dithionate-citrate
	Fe(II) (mg/g)	Fe(III) (mg/g)	Fe(II) (mg/g)	Fe(III) (mg/g)
Sediment	0.03	0.05	0.02	0.02
Red biofilm	0.10	0.24	0.02	0.21

24

Accepted Article

Legends

Fig. 1 The mats consisted of a thin red layer (1-2 mm) on top of coarse sand, (A) imaged from the side, and (B) from above. The bar in the (A) panel is 5 mm. The pore space in the sand underneath was filled with green biomass, consisting of mainly GSB. Beggiatoa are visible in the upper area of the right panel as thin white filaments. The arrow points towards a particularly densely populated area.

Fig. 2 Light attenuation spectra measured *in situ* using natural light (A) and using a halogen lamp producing white light (C). The light absorption spectra were calculated from the irradiance spectra measured at the mat surface and inside the mats at 0.5 mm steps with a 100 μm spherical irradiance sensor (Supplementary Information, Fig. S3). The irradiance data were integrated from 400-800 nm and used to plot total light attenuation *in situ* (B) and in the laboratory (D). The light absorption rates in 0.5 mm thick zones were obtained by dividing light spectrum at each depth by the one above. The numbers in the legend are the depths (m) of the lower spectra. (A) The upper layer (purple line) absorbs *in situ* much less light than the second layer (orange line). The enhanced absorption between 450 and 570 nm is due to accessory pigments, the maxima at 670 by Chl-a. Below 450 nm and above 700 nm the irradiance was too low to extract absorbance information. Similar maxima were observed by using white light (C), however, in addition the maxima at 810 nm by BChl became visible, due to the enhanced intensity in red light.

Fig. 3 A) Contour plot of 12 hour time series of oxygen profiles. B) The black continuous line presents the light level recorded at the lake bottom, the red continuous line represents the net photosynthesis rates as the sum of the oxygen fluxes, downward and upward from the concentration maximum.

Fig. 4 A) Contour plot of 12 hour time series of sulfide profiles. B) The continuous black line presents the light level recorded at the lake bottom, the red line represents the H_2S concentration at 1 cm depth.

Fig. 5 A) O_2 profiles and B) H_2S profiles measured *in situ* during midday (open symbols) and directly after sunset (closed symbols). The plots represent the average of 5 profiles. The oxygen production rates (R) calculated from A) are plotted in C). Negative values are respiration, positive values are net photosynthesis (when the sum of all oxygen consumptions is smaller than the local production). As no pH profiles were measured, sulfide conversion rates could not be calculated.

Fig. 6 Ex-situ Profiles of O_2, pH and S_{tot} measured in the dark (A) and under white light at 60 µmol photons $m^{-2}s^{-1}$ (B). The mat was incubated in natural spring water without added sulfide. S_{tot} was calculated from local H_2S and pH levels. The distribution of the consumption rates of O_2 and S_{tot}, calculated from their profiles, are plotted in C) and D).

Fig. 7 Ex-situ profiles of O_2, pH and H_2S measured in the dark (A) and in white light (B) at 60 µmol photons/m^2s. S_{tot} was calculated from local H_2S and pH levels. (C) Replicate profiles show that sulfide did not fully penetrate into the mats, in the dark with artificially enhanced sulfide levels in the water column.

Fig. 8 Dark-light shifts as measure for gross anoxygenic photosynthesis (GP). Upon illumination sulfide consumption commenced after ca 30 s (see Fig 10), the maximum rates were used as measure for gross photosynthesis rates. Also plotted are local sulfide production rates (continuous line A) determined from local increase upon darkening after long light exposure (B). The first profile upon darkening is indicated by S, the last by E, the last 3 profiles were used to calculate the local production rates.

Anbar, A.D., Duan1, Y., Lyons, T.W., Arnold, G.L., Kendall, B., Creaser, R.A. et al. (2007) A Whiff of Oxygen Before the Great Oxidation Event? *Science* **317**: 1903-1906.

Bateson, M.M., and Ward, D.M. (1988) Photoexcretion and fate of glycolate in a hot spring cyanobacterial mat. *Appl Environ Microbiol* **54**: 1738-1743.

Berg, H.C. (1983) *Random walks in biology.* Princeton, New Jersey: Princeton University Press.

Brune, D.C. (1989) Sulfur oxidation by phototrophic bacteria. *BBA-Bioenergetics* **975**: 189-221.

Canfield, D.E. (1998) A new model for Proterozoic ocean chemistry. *Nature* **396**: 450-453.

Canfield, D.E. (2013) *Oxygen: A Four Billion Year History* Princeton: Princeton University Press

Canfield, D.E., and Des Marais, D.J. (1991) Aerobic sulfate reduction in microbial mats. *Science* **251**: 1471-1473.

Canfield, D.E., and Teske, A. (1996) Late proterozoic rise in atmospheric oxygen concentration inferred from phylogenetic and sulphur-isotope studies. *Nature* **382**: 127-132.

Clausen, C.J., Cohen, A.D., Emiliani, C., Holman, J.A., and Stipp, J.J. (1979) Little Salt Spring, Florida: A Unique Underwater Site. *Science* **203**: 609-614.

Croce, R., and van Amerongen, H. (2014) Natural strategies for photosynthetic light harvesting. *Nature Chemical Biology* **10**: 492–501.

de Beer, D., Schramm, A., Santegoeds, C.M., and Kühl, M. (1997) A nitrite microsensor for profiling environmental biofilms. *Appl Environ Microbiol* **63**: 973-977.

Falkowski, P.G., and Raven, J.A. (2007) *Aquatic Photosynthesis (second edition)*: Princeton University Press.

Ferris, M.J., Nold, S.C., Revsbech, N.P., and Ward, D.M. (1997) Population structure and physiological changes within a hot spring microbial mat community following disturbance. *Appl Environ Microbiol* **63**: 1367-1374.

Findlay, A.J., Bennett, A.J., Hanson, T.E., and Luther III, G.W. (2015) Light-dependant sulfide oxidation in the anoxic zone of the Chesapeake Bay can be explained by small populations of phototrophic bacteria. *Appl Environ Microbiol* **81**: 7560-7569.

Gieseke, A., and de Beer, D. (2004) Use of microelectrodes to measure *in situ* microbial activities in biofilms, sediments, and microbial mats. In *Molecular Microbial Ecology Manual*. Akkermans, A.D.L., and van Elsas, D. (eds). Dordrecht (Nl): Kluwer, pp. 1581-1612.

Glazer, A.N. (1985) Light harvesting by phycobilisomes. *Ann RevBiophys Biophys Chem* **14**: 47-77.

Habicht, K., and Canfield, D.E. (1996) Sulphur isotope fractionation in modern microbial mats and the evolution of the sulphur cycle. *Nature* **382**: 342-343.

Hamilton, T.L., Bryant, D.A., and Macalady, J.L. (2016a) The role of biology in planetary evolution: cyanobacterial primary production in low-oxygen Proterozoic oceans. *Environm Microbiol* **18**: 325–340.

Hamilton, T.L., Welander, P., Albrecht, H.L., Fulton, J.M., Schaperdoth, I., Yang, E.S. et al. (2016b) Microbial communities and organic biomarkers in a Proterozoic-analog sinkhole environment. *Geobiology*: submitted.

Harada, J., Saga, Y., Oh-oka, H., and Tamiaki, H. (2005) Different sensitivities to oxygen between two strains of the photosynthetic green sulfur bacterium *Chlorobium vibrioforme* NCIB 8327 with bacteriochlorophyll c and d. *Photosynthesis Research* **86**: 137–143.

Henkel, S., Kasten, S., Poulton, S.W., and Staubwasser, M. (2016) Determination of the stable iron isotopic composition of sequentially leached iron phases in marine sediments. *Chemical Geology* **421**: 93–102.

Hoehler, T.M., Albert, D.B., Alperin, M.J., Bebout, B., Martens, C.S., and Des Marais, D. (2002) Comparative ecology of H_2 cycling in sedimentary and phototrophic ecosystems. *Ant v Leeuwenhoek* **81**: 575-585.

Imhoff, J.F. (2014) *Biology of Green Sulfur Bacteria*. Chichester: John Wiley & Sons,.

Jeroschewski, P., Steukart, C., and Kühl, M. (1996) An amperometric microsensor for the determination of H_2S in aquatic environments. *Anal Chem* **68**: 4351-4357.

Jørgensen, B.B., and Des Marais, D.J. (1988) Optical properties of benthic photosynthetic communities: Fiber-optic studies of cyanobacterial mats. *Limnol Oceanogr* **33**: 99-113.

Klatt, J.M. (2015) Photosynthesis and sulfur oxidation in microbial mats, unravelling the role of versatile Cyanobacteria in ancient ocean analogues. In *PhD thesis*: University of Bremen.

Knoll, A.H., Summons, R.E., Waldbauer, J.R., and Zumberge, J.E. (2007) The geological succession of primary producers in the oceans. In *The Evolution of Primary Producers in the Sea*. P., F., and Knoll, A.H. (eds). Boston: Academic Press, pp. 133–164.

Levenspiel, O. (1972) *Chemical reaction engineering*. New York: John Wiley & sons.

Liu, Z., Klatt, C.G., Ludwig, M., Rusch, D.B., Jensen, S.I., Kühl, M. et al. (2012) 'Candidatus Thermochlorobacter aerophilum:' an aerobic chlorophotoheterotrophic member of the phylum Chlorobi defined by metagenomics and metatranscriptomics. *ISME J* **6**: 1869–1882.

McConnell, M.C., Koop, R., Vasil'ev, S., and Bruce, D. (2002) Regulation of the Distribution of Chlorophyll and Phycobilin-Absorbed Excitation Energy in Cyanobacteria. A Structure-Based Model for the Light State Transition. *Plant Physiol* **130**: 1201–1212.

Millero, F.J., Plese, T., and Fernandez, M. (1988) The dissociation of hydrogen sulfide in seawater. *Limnol Oceanogr* **33**: 269-274.

Nichols, K.E., and Bogorad, L. (1962) Action Spectra Studies of Phycocyanin Formation in a Mutant of Cyanidium caldarium. *Botanical Gazette* **124**: 85-93.

Nielsen, L.P., Risgaard-Pedersen, N., Fossing, H., Christensen, P.B., and Sayama, M. (2010) Electric currents couple spatially separated biogeochemical processes in marine sediment. *Nature* **463**: 1071-1074.

Nübel, U., Bateson, M.M., Vandieken, V., Wieland, A., Kühl, M., and Ward, D.A. (2002) Microscopic examination of distribution and phenotypic properties of phylogenetically diverse *Chloroflexaceae*-related bacteria in hot spring microbial mats. *Appl Environm Microbiol* **68**: 4593-4603.

Oren, A., Padan, E., and Avron, M. (1977) Quantum yields for oxygenic and anoxygenic photosynthesis in the cyanobacterium Oscillatoria limnetica. *PNAS* **74**: 2152-2156.

Overmann, J., and Garcia-Pichel, F. (2012) The phototrophic way of life. In *Prokaryotes*. Rosenberg, E. (ed). Berlin, Heidelberg: Springer, pp. 203-257.

Overmann, J., Cypionka, H., and Pfennig, N. (1992) An extremely low-light-adapted phototrophic sulfur bacterium from the Black Sea. *Limnol Oceanogr* **37**: 150–155.

Preisler, A., de Beer, D., Lichtschlag, A., Lavik, G., Boetius, A., and Jørgensen, B.B. (2007) Biological and chemical sulfide oxidation in a *Beggiatoa* inhabited marine sediment. *ISME-Journal* **1**: 341-353.

Raiswell, R., Canfield, D.E., and Berner, R.A. (1994) A comparison of iron extraction methods for the determination of degree of pyritisation and the recognition of iron-limited pyrite formation. *Chemical Geology* **111**: 101-110.

Ramsing, N.B., Ferris, M.J., and Ward, D.M. (2000) Highly ordered vertical structure of Synechococcus populations within the one-millimeter-thick photic zone of a hot spring cyanobacterial mat. *Appl Environm Microbiol* **66**: 1038-1049.

Revsbech, N.P., and Ward, D.M. (1983) Oxygen microelectrode that is insensitive to medium chemical composition: Use in an acid microbial mat dominated by *Cyanidium caldarum. Appl Environ Microbiol* **45**: 755-759.

Rickelt, L.F., Lichtenberg, M., Trampe, E.C.L., and Kuhl, M. (2016) Fiber-Optic Probes for Small-Scale Measurements of Scalar Irradiance. *Photochemistry and Photobiology* **92**: 331–342.

Stolz, F., and Margulis, L. (1984) The stratified microbial community at Laguna Figueroa, Baja California, Mexico: A possible model for prephanerozoic laminated microbial communities preserved in cherts. *Origins of Life and Evolution of Biospheres* **14**: 671-679.

Stomp, M., Huisman, J., Stal, L.J., and Matthijs, H.C.P. (2007) Colorful niches of phototrophic microorganisms shaped by vibrations of the water molecule. *ISME J* **1**: 271–282.

van Gemerden, H. (1984) The sulfide affinity of phototrophic bacteria in relation to the location of elemental sulfur. *Arch Microbiol* **39**: 289-294.

Voorhies, A.A., Eisenlord, S.D., Marcus, D.N., Duhaime, M., Bopaiah A. Biddanda, B.A., Cavalcoli, D., and Dick, G.J. (2016) Ecological and genetic interactions between cyanobacteria and viruses in a low-oxygen mat community inferred through metagenomics and metatranscriptomics. *Environmental Microbiology* **18**: 358–371.

Wangpraseurt, D., Polerecky, L., Larkum, A.W.D., Ralph, P.J., Nielsen, D.A., Pernice, M., and Kuhl, M. (2014) The *in situ* light microenvironment of corals. *Limnol Oceanogr* **59**: 917–926.

Weber, M., Faerber, P., Meyer, V., Lott, C., Eickert, G., Fabricius, K.E., and de Beer, D. (2007) *In situ* applications of a new diver-operated motorized microsensor profiler. *Env Sci Technol* **41**: 6210-6215.

Wieland, A., and Kühl, M. (2000) Irradiance and temperature regulation of oxygenic photosynthesis and O_2 consumption in a hypersaline cyanobacterial mat (Solar Lake, Egypt). *Mar Biol* **137**: 71-85.

Wieland, A., Zopfi, J., Benthien, M., and Kühl, M. (2005) Biogeochemistry of an iron-rich hypersaline microbial mat (Camargue, France). *Microb Ecol* **49**: 34-49.

Wieland, A., de Beer, D., van Dusschoten, D., Damgaard, L.R., Kühl, M., and van As, H. (2001) Fine-scale measurement of diffusivity in a microbial mat with NMR imaging. *Limnol Oceanogr* **44**: 248-259.

Zarikian, C.A.A., Swart, P.K., Gifford, J.A., and Blackwelder, P.L. (2005) Holocene paleohydrology of Little Salt Spring, Florida, based on ostracod assemblages and stable isotopes. *Palaeogeography, Palaeoclimatology, Palaeoecology* **225**: 134–156.

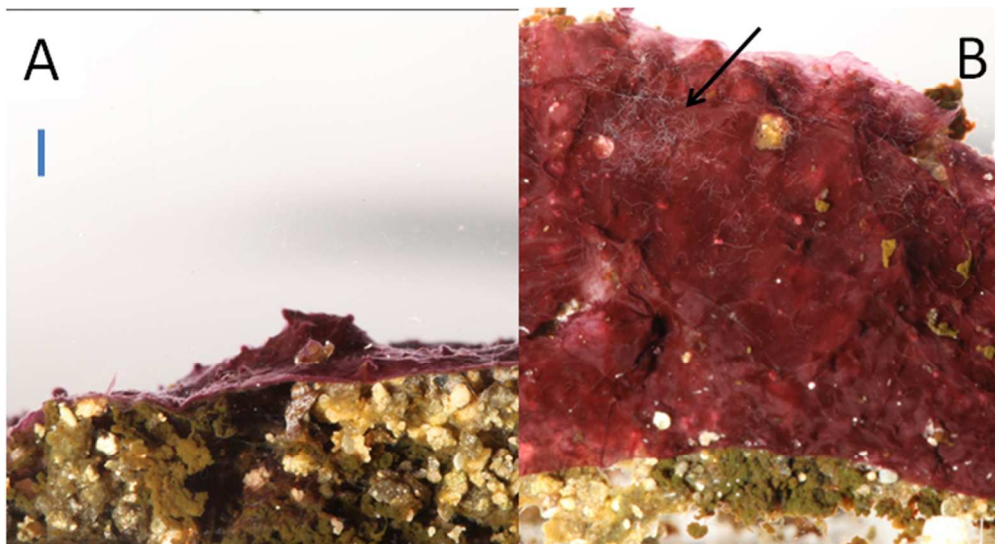|	HCl-extraction		Na-acetate	dithionate-citrate
	Fe(II) (mg/g)	Fe(III) (mg/g)	Fe(II) (mg/g)	Fe(III) (mg/g)
Sediment	0.03	0.05	0.02	0.02
Red biofilm	0.10	0.24	0.02	0.21

Accepted Article

Fig. 1 The mats consisted of a thin red layer (1-2 mm) on top of coarse sand, (A) imaged from the side, and (B) from above. The bar in the (A) panel is 5 mm. The pore space in the sand underneath was filled with green biomass, consisting of mainly GSB. Beggiatoa are visible in the upper area of the right panel as thin white filaments. The arrow points towards a particularly densely populated area.

257x141mm (72 x 72 DPI)

Fig. 2 Light attenuation spectra measured in situ using natural light (A) and using a halogen lamp producing white light (C). The light absorption spectra were calculated from the irradiance spectra measured at the mat surface and inside the mats at 0.5 mm steps with a 100 μm spherical irradiance sensor (Supplementary Information, Fig. S3). The irradiance data were integrated from 400-800 nm and used to plot total light attenuation in situ (B) and in the laboratory (D). The light absorption rates in 0.5 mm thick zones were obtained by dividing light spectrum at each depth by the one above. The numbers in the legend are the depths (m) of the lower spectra. (A) The upper layer (purple line) absorbs in situ much less light than the second layer (orange line). The enhanced absorption between 450 and 570 nm is due to accessory pigments, the maxima at 670 by Chl-a. Below 450 nm and above 700 nm the irradiance was too low to extract absorbance information. Similar maxima were observed by using white light (C), however, in addition the maxima at 810 nm by BChl became visible, due to the enhanced intensity in red light.
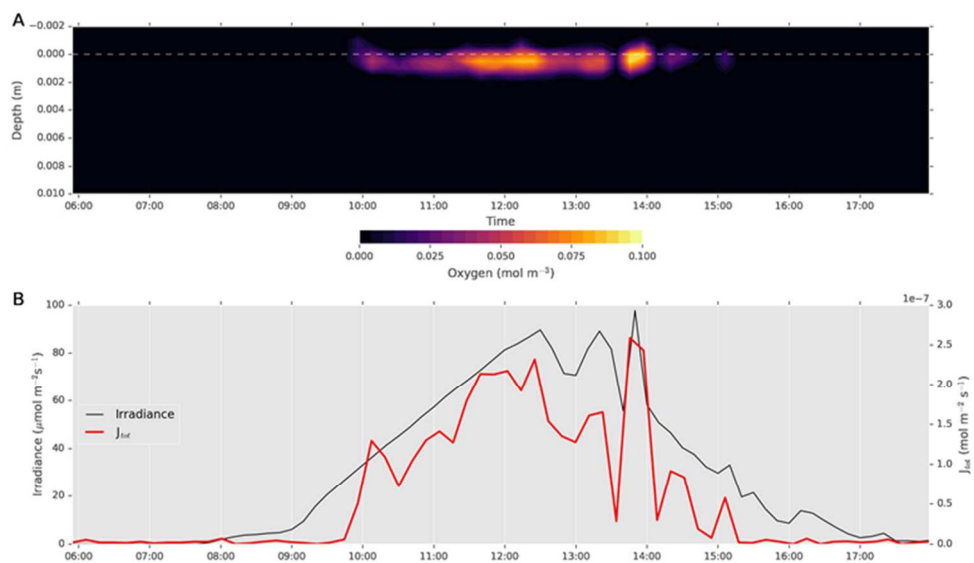
252x265mm (72 x 72 DPI)

Fig. 3 A) Contour plot of 12 hour time series of oxygen profiles. B) The black continuous line presents the light level recorded at the lake bottom, the red continuous line represents the net photosynthesis rates as the sum of the oxygen fluxes, downward and upward from the concentration maximum.
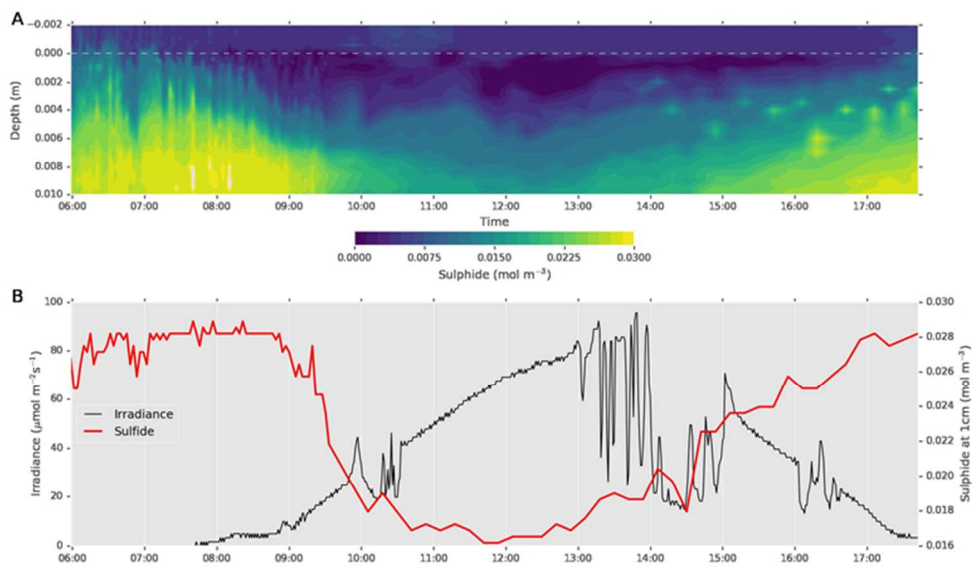
281x167mm (72 x 72 DPI)

Fig. 4 A) Contour plot of 12 hour time series of sulfide profiles. B) The continuous black line presents the light level recorded at the lake bottom, the red line represents the H2S concentration at 1 cm depth.

280x165mm (72 x 72 DPI)
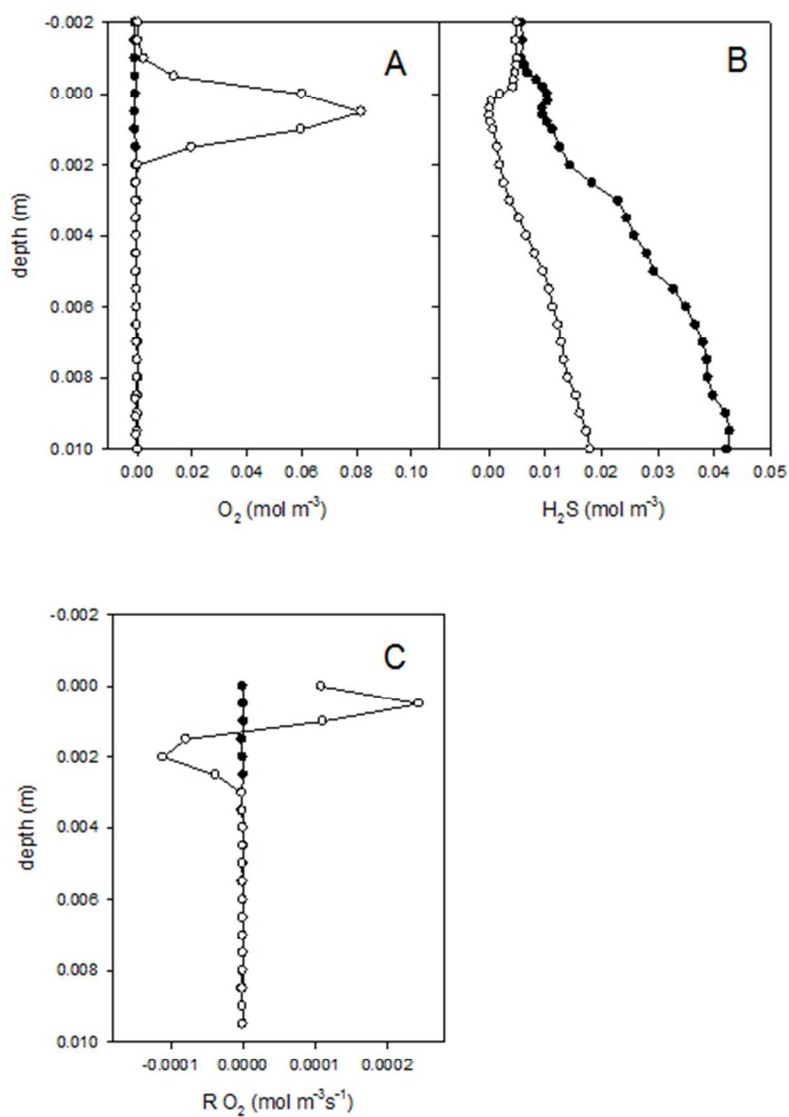
Fig. 5 A) O2 profiles and B) H2S profiles measured in situ during midday (open symbols) and directly after sunset (closed symbols). The plots represent the average of 5 profiles. The oxygen production rates (R) calculated from A) are plotted in C). Negative values are respiration, positive values are net photosynthesis (when the sum of all oxygen consumptions is smaller than the local production). As no pH profiles were measured, sulfide conversion rates could not be calculated.
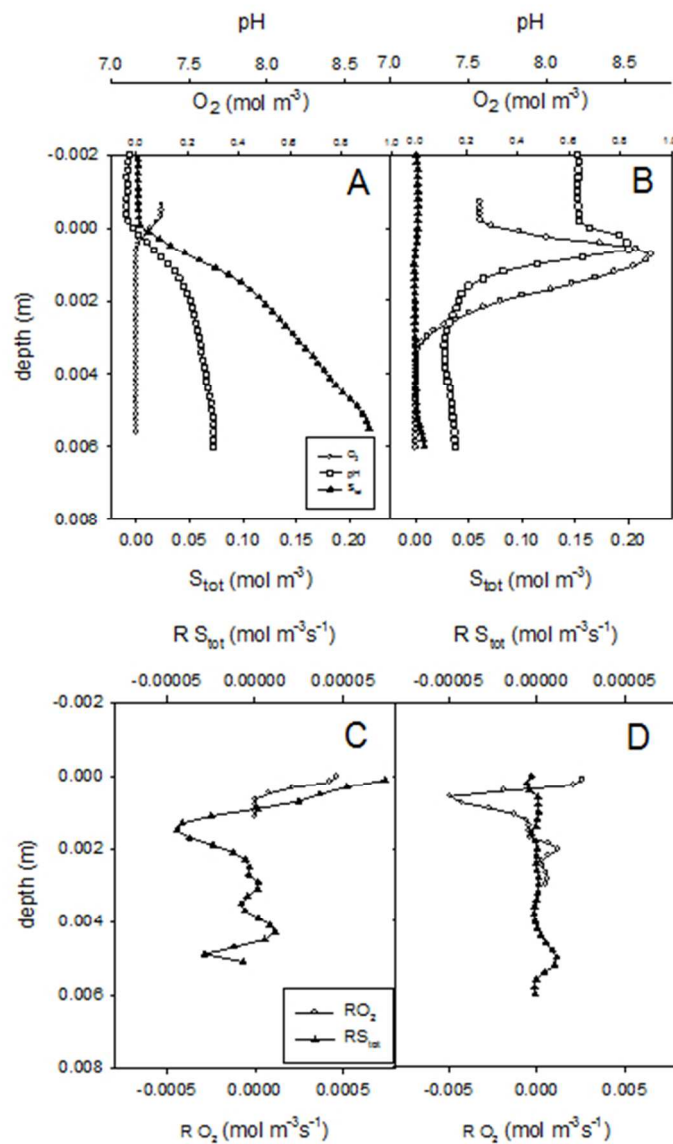
184x252mm (72 x 72 DPI)

Fig. 6 Ex-situ Profiles of O2, pH and Stot measured in the dark (A) and under white light at 60 μmol photons m-2s-1 (B). The mat was incubated in natural spring water without added sulfide. Stot was calculated from local H2S and pH levels. The distribution of the consumption rates of O2 and Stot, calculated from their profiles, are plotted in C) and D).
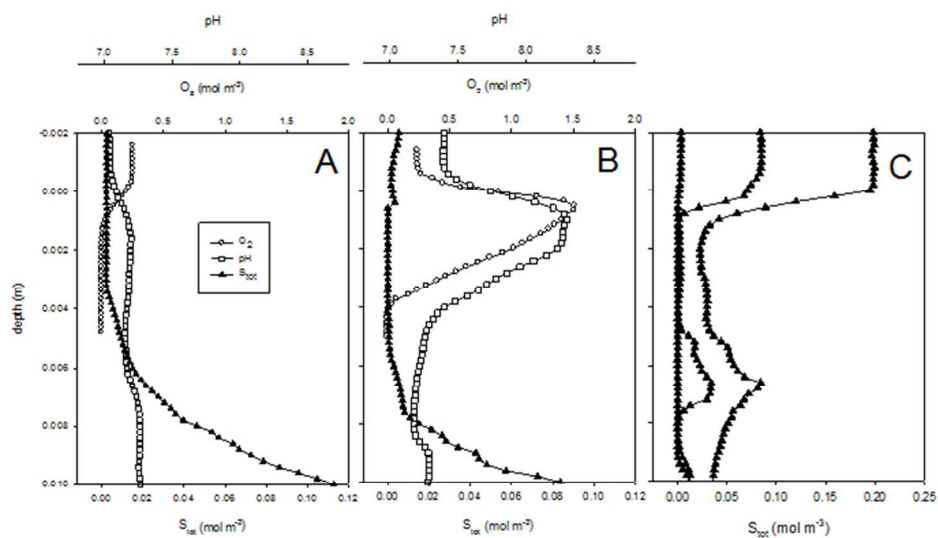
153x243mm (72 x 72 DPI)

Fig. 7 Ex-situ profiles of O2, pH and H2S measured in the dark (A) and in white light (B) at 60 μmol photons/m2s. Stot was calculated from local H2S and pH levels. (C) Replicate profiles show that sulfide did not fully penetrate into the mats, in the dark with artificially enhanced sulfide levels in the water column.
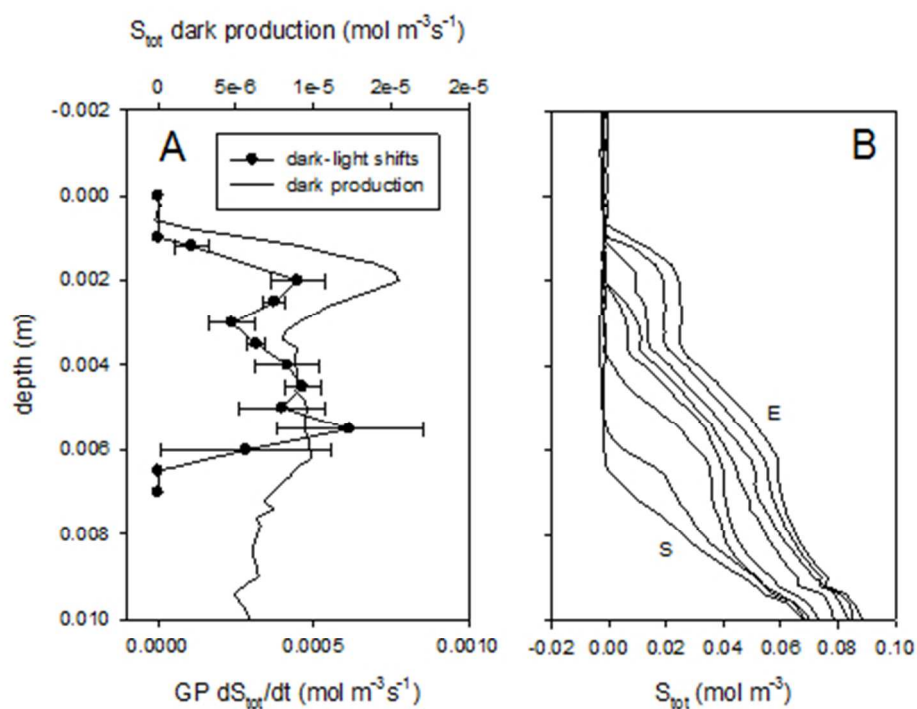
258x151mm (72 x 72 DPI)

Fig. 8 Dark-light shifts as measure for gross anoxygenic photosynthesis (GP). Upon illumination sulfide consumption commenced after ca 30 s (see Fig 10), the maximum rates were used as measure for gross photosynthesis rates. Also plotted are local sulfide production rates (continuous line A) determined from local increase upon darkening after long light exposure (B). The first profile upon darkening is indicated by S, the last by E, the last 3 profiles were used to calculate the local production rates.

171x132mm (72 x 72 DPI)